Polarized Light Absorption in Wurtzite InP Nanowire Ensembles

ARTICLE *in* NANO LETTERS · JANUARY 2015

Impact Factor: 13.59 · DOI: 10.1021/nl5038374 · Source: PubMed

NANO LETTERS

Letter

pubs.acs.org/NanoLett

Polarized Light Absorption in Wurtzite InP Nanowire Ensembles

Marta De Luca,[†] Attilio Zilli,[†,⊥] H. Aruni Fonseka,[‡] Sudha Mokkapati,[‡] Antonio Miriametro,[†] Hark Hoe Tan,[‡] Leigh Morris Smith,[‡,§] Chennupati Jagadish,[‡] Mario Capizzi,[†] and Antonio Polimeni*[,†]

[†]Dipartimento di Fisica and CNISM, Sapienza Università di Roma, Piazzale A. Moro 2, 00185 Roma, Italy

[‡]Department of Electronic Materials Engineering, Research School of Physics and Engineering, The Australian National University, Canberra, Australian Capital Territory, 0200, Australia

[§]Department of Physics, University of Cincinnati, Cincinnati, Ohio 45221, United States

Supporting Information

ABSTRACT: We investigate the absorption properties of ensembles of wurtzite (WZ) InP nanowires (NWs) by high-resolution polarization-resolved photoluminescence excitation (PLE) spectroscopy at T = 10 K. The degree of linear polarization of absorbed light, ρ_{abs}, resulting from the PLE spectra is governed by a competition between the dielectric mismatch effect and the WZ selection rules acting differently on different optical transitions. These two contributions are deconvoluted with the help of finite-difference time-domain simulations, thus providing information about the symmetry of the three highest valence bands (A, B, and C) of WZ InP and the extent of the spin−orbit interaction on these states. Moreover, ρ_{abs} shows two characteristic dips corresponding to the two sharp A and B exciton resonances in the PLE spectra. A model developed for the dip in A provides the first experimental evidence of an enhancement in the dielectric mismatch effect originating from the Coulomb interaction between electron and hole.

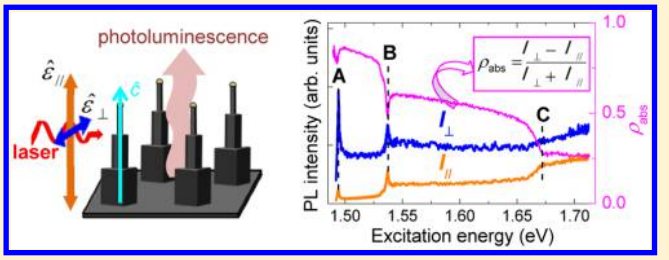

KEYWORDS: *InP nanowires, photoluminescence excitation, wurtzite band structure, dielectric mismatch, excitons*

INTRODUCTION

The tremendous interest attracted by semiconductor nanowires (NWs) among researchers and engineers is triggered by the great number of physical investigations and technological applications that these nanostructures enable.[1] On the one hand, *individual NWs* are promising building blocks for nanoscale integrated electronic and optoelectronic devices.[2,3] On the other hand, *NW ensembles* are gaining attention as a versatile and cost-effective option for applications such as energy conversion[4] and photovoltaics.[5] Specifically, the high efficiency/cost ratio of NW-based solar cells is due to NW ability to maximize light absorption and their possibility of being grown on inexpensive substrates, such as silicon.[6] Owing to the direct band gap that partly matches with the solar spectrum and low surface recombination velocity,[7] InP nanowires are excellent candidates among the III−V compound semiconductors for high-efficiency solar cells.[8]

Significant improvements in current device performance, as well as a clever design of new NW-based devices, must be driven by a deep understanding of the NWs' physical properties. One of the most intriguing findings in the fundamental characteristics of NWs is their polytypism, namely, the occurrence of several different crystal structures.[9] Many non-nitride III−V NWs have been grown in the wurtzite (WZ) phase, a phase unstable in the corresponding bulk crystals, which exhibit, instead, the ubiquitous zincblende (ZB) phase. Therefore, the band structure of several WZ III−V compounds has been intensively studied during the past few years.[10−14] Contrary to GaAs, where even the value of the band gap energy is still controversial,[15] the energy of the fundamental band gap and of higher-energy critical points in WZ InP have been well established by optical techniques.[16−27] The larger band gap peculiar to the WZ phase, as well as the high crystalline quality of WZ InP NWs, have recently made these nanostructures a stand out for NW array solar cells.[28,29]

In this work, we measure the dependence on absorbed light polarization of photoluminescence (PL) excitation (PLE) spectra in ensembles of InP WZ nanowires. The spectral dependence of the resulting absorption polarization degree, ρ_{abs}, combined with finite-difference time-domain calculations allows us to separate the *microscopic electronic anisotropy* inherent to the hexagonal point symmetry of WZ from the *macroscopic optical anisotropy* associated with the dielectric mismatch between the NWs and their environment. Thus, we determine with high accuracy the energy and the symmetry of the highest-energy valence bands (A, B, and C bands), assess the extent of the spin−orbit effect on these states, and explore the influence of finite k vectors on the selection rules for the optical transitions involving the fundamental band gap absorption. In addition, the measured absorption polarization-degree discloses the subtle, yet important role played by excitons on the NW optical dispersion.

Received: October 6, 2014
Revised: December 22, 2014

DOI: 10.1021/nl5038374
Nano Lett. XXXX, XXX, XXX−XXX

In contrast to present work, many past experimental works on WZ InP nanowires have addressed the polarization properties of light *emission*, therefore in an energy-range restricted to the band gap transition energy.[15,17,24,26,30] Moreover, most of the existing works rely on micro-photoluminescence (μ-PL) measurements on *single nanowires*.[17,23,24,26] We bring to view that (i) isolated NWs transferred onto a substrate undergo changes in their dielectric environment, which modifies the optical properties with respect to the free-standing NWs, as it will be discussed later; (ii) the high numerical-aperture microscope objectives used for μ-PL alter light polarization in a complicated way; (iii) single NW studies do not allow for the observation of collective light absorption mechanisms that typically occur in NW ensembles[31−33] and often depend on ensemble parameters, such as NW spacing. Therefore, conclusions drawn from the characterization of single NWs may not apply to as-grown ensembles of vertical NWs, as those used in solar cells and photodetectors. Recently, polarized photoexcitation measurements on ensembles of vertical wurtzite InP NWs have been performed,[34] but neither polarization selectivity nor energy dependence of the polarized light absorption was reported. Finally, differential polarized reflectance was exploited in photomodulated Rayleigh scattering measurements[20] to estimate the A, B, and C band gap energies, but no information was provided on the sign of the reflectance difference between parallel and orthogonal polarization of the light incident on the NW.

SAMPLE AND EXPERIMENTAL DETAILS

The samples we have investigated are wurtzite InP NWs grown by Au-catalyzed metal−organic chemical vapor deposition, at a temperature of 480 °C and V/III ratio of 350, on semi-insulating InP (111)B substrates.[26,35] This growth yielded a high density (~8 NWs/μm^2) of vertical, ~1 μm long wires, as shown in the 45° tilt scanning electron microscopy (SEM) image in Figure 1a. The NWs are parallel to each other and similar in size and shape. The top view of a single wire in the inset shows the hexagonal-truncated triangular cross section typically seen in NWs grown in ⟨111⟩ direction. The NWs feature a staggered structure, which can be approximated by a base (length ~400 nm) with 180 nm side triangular cross section, followed by a segment (length ~400 nm) with a 60 nm side hexagonal cross section and a tip (length ~200 nm) with 15 nm side hexagonal cross section with a gold nanoparticle on top. These sizes allow us to rule out sizable quantum confinement effects, at least in most of the NW volume.[36] The NW shape does not influence the optical properties of the NWs that are related to the NW hexagonal point symmetry. As a matter of fact, other samples with WZ phase but diverse morphologies all show a predominant polarization of the emitted light directed perpendicular to the NW $\hat{c}$ axis. Here, we have chosen the sample exhibiting the best optical properties in terms of luminescence efficiency and line width. Incidentally, a tapered shape has been demonstrated to maximize absorption in InP NW arrays (98% against 45% in cylindrical NWs, if efficiency is not normalized to the material volume)[37] and in Ge nanopillar arrays (simultaneously minimizing reflectance, in this case).[38] Also, tapering should endow the NWs with a robust structure, enabling them to preserve the ensemble orientation against bending caused by charging and capillary effects that could occur during postgrowth processing or during exposure to laser in optical measurements. The transmission electron microscopy (TEM) image of a nanowire is displayed in Figure 1b, where extended planar defects are seen only in the tip region. The high-resolution close-up in Figure 1c reveals pure WZ crystal structure with the $\hat{c}$ axis aligned with the NW symmetry axis. Finally, the good crystalline quality of the WZ lattice is also confirmed by the selected-area diffraction pattern shown in Figure 1d.

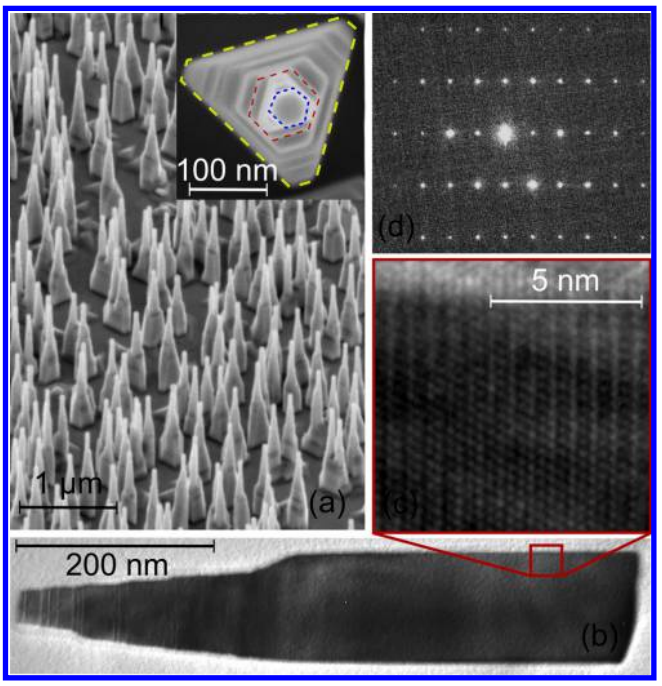

Figure 1. Microscopic characterization of the InP NW sample. (a) 45° tilt SEM image of the InP NW ensemble. Inset: Top view SEM image of a single NW. The NW shape can be approximated to a staggered structure consisting of the three parts highlighted by differently colored lines. (b) TEM micrograph of a single NW (planar defects are observed only in the tip region). (c) High-resolution TEM image of the region indicated by the red square and (d) a selected-area diffraction pattern taken along the [11-20] zone axis from the middle region of the nanowire shown in (b). Both images demonstrate pure WZ crystal structure.

We have investigated the photon−energy dependence of the polarized light absorbed by the NWs by polarization-resolved PLE. In a typical PLE experiment, PL emission is recorded at a fixed energy as a function of the excitation energy. Therefore, under some assumptions, a PL excitation spectrum is equivalent to an absorption spectrum.[39] PLE is a technique particularly suitable for studying absorption mechanisms in nanostructure ensembles[15,18,19,33] where standard transmission measurements would be challenging due to a prevailing absorption from the substrate. Here, PL and PLE measurements were performed on NW ensembles in a grazing incidence configuration by using a continuous-wave Ti:sapphire tunable laser as the excitation source, as illustrated in Figure 2.

A liquid crystal variable retarder, set at $\lambda/2$ retardance, was inserted in the exciting beam path in order to switch electronically between parallel ($\hat{\varepsilon}_{\parallel}$) and perpendicular ($\hat{\varepsilon}_{\perp}$) laser polarization with respect to the NW $\hat{c}$ axis while keeping the excitation wavelength fixed. The laser beam was carefully focused onto the sample by a 10 cm focal length lens resulting in a spot with ~100 μm transverse section and depth of focus of about 10 mm. A He closed-cycle cryostat maintained the sample temperature at 10 K. The sample emission was collected along the wire axis. The PL signal was dispersed by a 1.5 m

DOI: 10.1021/nl5038374
Nano Lett. XXXX, XXX, XXX−XXX

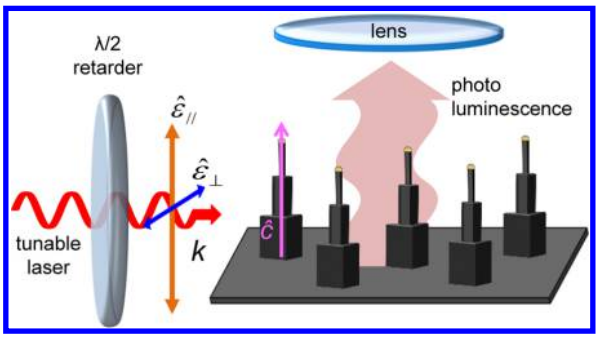

Figure 2. Schematic of the experimental setup used for polarization-resolved PLE measurements. The NW ensemble is excited by a Ti:sapphire laser in grazing incidence illumination, namely, with laser wave vector $\boldsymbol{k}$ perpendicular to the WZ $\hat{c}$ axis (which coincides with the NW symmetry axis). A liquid crystal variable retarder set at $\lambda/2$ retardance allows switching between a light polarization vector either parallel ($\hat{\varepsilon}_{\parallel}$) or perpendicular ($\hat{\varepsilon}_{\perp}$) to the $\hat{c}$ axis. Luminescence emitted by the NW ensemble for each laser polarization is collected along the wire axis and steered to a monochromator by a lens system.

focal length double monochromator equipped with a 600 grooves/mm grating and detected by either a liquid N-cooled Si CCD for PL or a Peltier-cooled GaAs photomultiplier for PLE (detection bandwidth equal to 0.2 meV). For each excitation wavelength, the PL signals for $\hat{\varepsilon}_{\perp}$ and $\hat{\varepsilon}_{\parallel}$ were acquired one after the other with a 0.5 s delay and the wavelength and power of the scanning laser were automatically recorded by a Michelson interferometer (resolution equal to 0.02 nm) and a calibrated Si power meter, respectively.

RESULTS AND DISCUSSION

Polarization-Resolved Photoluminescence Excitation. Figure 3a and b show some representative PL spectra recorded at T = 10 K by exciting the NW ensemble with laser polarized parallel or perpendicular to the NW symmetry axis. The only difference between the two panels is the exciting photon energy (E_{exc}), which is equal to 1.521 and 1.589 eV in Figure 3a and b, respectively. Several contributions can be recognized in the spectra. The highest energy peak (1.493 eV) is due to the band gap free-exciton (FE) recombination, usually referred to as A exciton in WZ materials. Here, it shows a doublet structure, which may originate from bound excitons lying 1 meV below the FE or be due to FE-polariton scattering by various mechanisms.[40,41] The other low-energy features can be ascribed to point or line defects, as suggested by their dependence on power and temperature and are discussed in more detail in paragraph S1 of the Supporting Information.[26]

In panel a, the emitted luminescence is much more intense when excited by perpendicular rather than by parallel polarized light. This anisotropy is evaluated by the degree of linear polarization $\rho = (I_{\perp}^{PL} - I_{\parallel}^{PL})/(I_{\perp}^{PL} + I_{\parallel}^{PL})$, where $I_{\perp}^{PL}$ and $I_{\parallel}^{PL}$ are the PL intensities for an equal-intensity laser excitation either perpendicular or parallel to the NW $\hat{c}$ axis, respectively (we stress that the emitted PL is not polarization-resolved and only the exciting photons are). Panel c shows ρ as a function of the emitted photon energy for E_{exc} = 1.521 eV. ρ is positive over the total NW emission range, increases with increasing photon energy, and reaches its maximum value (~0.8) around the FE emission energy. The positive value of the absorption (or emission) degree of linear polarization around the band gap energy is distinctive of selection rules of A excitons in WZ phase materials.[15,17,24,26,30,42−44] In panel a the excitation energy was just above the band gap energy, while PL spectra in panel b result from the very same measurement taken for a higher excitation energy (~70 meV above the band gap energy). The PL signal excited by perpendicular polarized light is still more intense than that excited by parallel polarized light, but to a much lower extent in comparison with the previous case of near band gap excitation. For this higher excitation energy, ρ varies only from +0.1 to +0.3 with increasing emission energy, as displayed in panel d, thus exhibiting a rather different behavior with respect to that shown in panel c for a lower excitation energy. These results unambiguously highlight a different intensity of light absorption that depends on the polarization and energy of the exciting photons.

In order to further investigate that dependence, we performed high-resolution polarization-resolved PLE. The

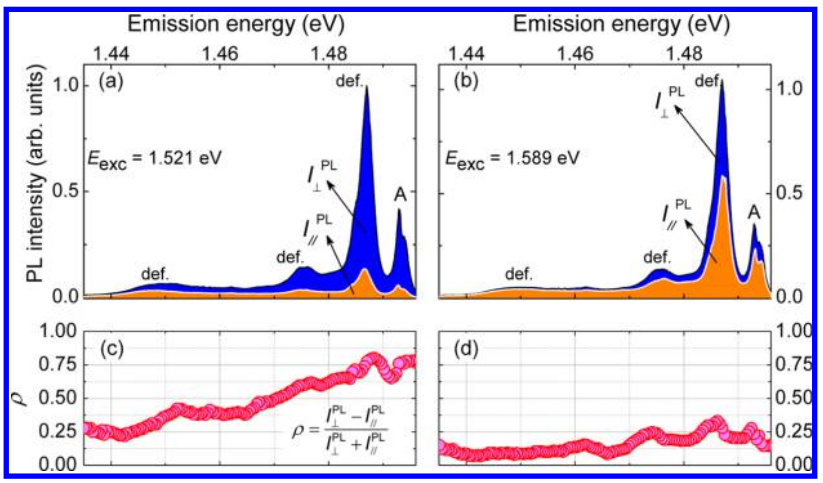

Figure 3. (a) PL spectra recorded at T = 10 K on an InP NW ensemble (E_{exc} = 1.521 eV; power density P = 0.25 W/cm^2). PL spectra excited by laser light polarized perpendicular and parallel to the NW $\hat{c}$ axis are colored in blue and orange, respectively. The origin of the different transitions is discussed in the text. (b) PL spectra as in (a) but excited with E_{exc} = 1.589 eV and P = 0.25 W/cm^2. "A" and "def." label the recombination of the free excitons of band A and transitions related to defects, respectively. (c) Degree of linear polarization ρ of PL excited by photons having polarization orthogonal ($I_{\perp}^{PL}$) and parallel ($I_{\parallel}^{PL}$) to $\hat{c}$ for the two spectra shown in (a), respectively. (d) Same as (c) for the two spectra shown in (b). Different excitation energies clearly yield significantly different photogenerated carrier density (i.e., absorption) and, consequently, ρ.

DOI: 10.1021/nl5038374
Nano Lett. XXXX, XXX, XXX−XXX

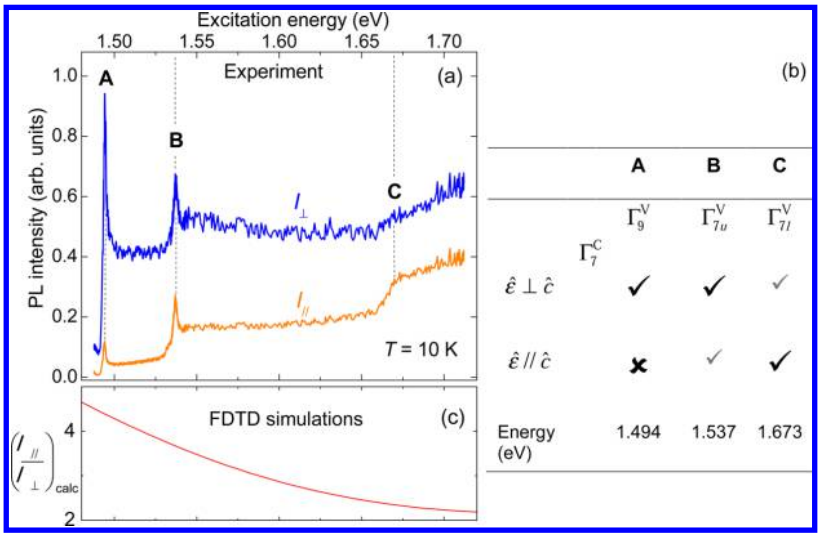

Figure 4. (a) PLE spectra taken at T = 10 K with detection energy set at 1.486 eV. The spectra were excited with light polarization vectors parallel (orange line, $I_{\parallel}$) or perpendicular (blue line, $I_{\perp}$) to the NW $\hat{c}$ axis and were recorded almost simultaneously. A, B, and C absorption edges are indicated, the latter being clearly visible only with parallel excitation. (b) Table of the optical selection rules in wurtzite materials for transitions A, B, and C from the three valence bands (with symmetries Γ_9^V, Γ_{7u}^V, and Γ_{7l}^V, respectively) to the bottommost conduction band (with symmetry Γ_7^C) for light polarization perpendicular or parallel to the WZ $\hat{c}$ axis (see refs 43 and 44). The black ticks (crosses) represent optically allowed (forbidden) transitions. Smaller gray ticks represent transitions allowed only by spin−orbit interaction. The energies measured for the A, B, and C transitions are given in the last row of the table. (c) Variation of the ratio $(I_{\parallel}/I_{\perp})_{calc}$ due to the dielectric mismatch effect as found by finite difference time-domain (FDTD) simulations.

anisotropy of the NW optical response is quantified by introducing the degree of linear polarization of the *absorbed* light

$$\rho_{abs} = \frac{I_{\perp} - I_{\parallel}}{I_{\perp} + I_{\parallel}} \quad (1)$$

where $I_{\perp}$ and $I_{\parallel}$ are now the *PLE intensities*—different, therefore, from the perpendicular and parallel polarized PL components usually measured in polarization-resolved emission experiments.[15,17,24,26,30] The detection was set at the defect peak at 1.486 eV (see Figure 3), whose emission displays the same degree of polarization shown by the FE band. The excitation energy was varied between 1.487 and 1.720 eV in steps of ∼0.2 meV (and ∼0.05 meV at the critical points). Figure 4a shows the resulting PLE spectra for $\hat{\varepsilon}_{\perp}$ and $\hat{\varepsilon}_{\parallel}$ laser excitations represented with blue and orange lines, respectively. We point out that the PLE spectra, and hence the absorption polarization degree, do not change considerably with PL detection energy, as shown in Figure S2 in the Supporting Information. We first comment on the main features of the PLE spectra and then on their dependence on the exciting photon polarization. Both PLE spectra present three step-like absorption edges corresponding to the A, B, and C optical transitions typical of the WZ band structure.[10] These transitions involve the bottommost conduction band minimum, with Γ_7^C symmetry, and the three valence band maxima, with Γ_9^V, Γ_{7u}^V, and Γ_{7l}^V symmetry (in order of increasing hole energy), labeled as A, B, and C, in the order (see Figure 4b). At T = 10 K, we find E_A = 1.494 eV (the 1 meV difference with respect to the PL peak energy is due to the Stokes shift between absorption and emission),[45] E_B = 1.537 eV, and E_C = 1.673 eV. In turn, the resulting spin−orbit and crystal field splittings, as calculated in the quasicubic approximation,[12] are Δ_{so} = 86 meV and Δ_{cr} = 138 meV, respectively. These quantities do not depend on the polarization of exciting light or on the detection energy (see Figure S2a in the Supporting Information). A and B absorption edges also exhibit remarkably sharp excitonic features (line width ∼2 meV) which, along with the high radiative efficiency observed, testify the excellent optical quality of the sample. In turn, this allows us to establish with great accuracy the energies of A, B, and C transitions. In the current literature, these energy values fall within a rather wide range, with A varying between 1.486 and 1.508 eV, B between 1.530 and 1.539 eV, and C between 1.665 and 1.690 eV, as determined by various optical techniques.[17−27,34] Some of these values are in agreement with ours, but our spectral quality is unprecedented. As a matter of fact, our spectral resolution and sample quality enable us to observe subtle peculiar features not previously reported, as will be detailed later.

We now discuss the effect of light polarization on the PLE spectra. The A exciton shows a much more intense absorption of perpendicular polarized light with respect to parallel polarized light ($I_{\perp}/I_{\parallel} \sim 9$). We notice that the variation of this value is small up to the B resonance (E < 1.530 eV), thus indicating that the absorption anisotropy is preserved also for $k \neq 0$ (or continuum) transitions. The estimate of $I_{\perp}/I_{\parallel}$ for transition B is nontrivial because of the underlying contribution from $k \neq 0$ transitions associated with band A that extend to the energy of transition B and beyond. Therefore, a sensible background subtraction has to be performed, as explained in Section S3 of the Supporting Information. As a result of that subtraction, band B and its continuum (1.537 eV< E < 1.670 eV) now display a comparable intensity for the two light polarizations with $I_{\perp}/I_{\parallel} \sim 1.4$ at the B resonance. At and above the C transition (E > 1.670 eV), absorption occurs mainly for parallel light polarization ($I_{\perp}/I_{\parallel} \sim 0.3$ at the C edge after subtraction of the contributions from A and B continua; see Figure S3 in the Supporting Information). Recent PLE measurements on single WZ InP NWs showed results that are partially opposite to those reported here.[23] We attribute these differences to a different experimental configuration in

DOI: 10.1021/nl5038374
Nano Lett. XXXX, XXX, XXX−XXX

which a single NW lying on the substrate was measured through an objective.

The large size of our NWs rules out any sizable quantization effect. Therefore, the energy-dependent anisotropy in the optical absorption seen in our measurements can be accounted for only by two competing mechanisms.

(i) The first one is related to the *microscopic anisotropy* of the hexagonal crystal lattice, implying a preferred direction given by the $\hat{c}$ axis. Such anisotropy, which is independent of the NW macroscopic shape, is responsible for the selection rules summarized in Figure 4b for the three lowest-energy optical transitions A, B, and C.[44,46] For perpendicular polarized light, A and B transitions are fully allowed, whereas C is allowed only by the spin−orbit coupling. For parallel polarized light, C is fully allowed, whereas B is allowed only by spin−orbit coupling and A is forbidden.[46] As a consequence of these selection rules, $I_\perp/I_\parallel$ should be at a maximum only when transitions from the A band are considered and then drop when higher energy and less or oppositely polarized transitions are activated. In fact, a sizable spin−orbit perturbation may result in a much smaller polarization (smaller $I_\perp/I_\parallel$ ratio, but >1) for transition B, and even in an inverse polarization for transition C (i.e., $I_\perp/I_\parallel < 1$). Therefore, the different intensities of B and C transitions when excited by light of different polarizations can provide valuable experimental information on the strength of the spin−orbit interaction in WZ materials that has only been addressed theoretically in a few reports.[14,46]

(ii) The second mechanism is related to the *macroscopic anisotropy* associated with the elongated shape of the NWs, regardless of the crystal phase. According to electrostatic calculations (namely, in the limit of wavelengths much greater than the NW radius),[47] the mismatch in dielectric constants between a cylinder (i.e., a NW assumed to have infinite length) and its surroundings (here, the vacuum) muffles the perpendicular component of an applied electric field within the wire, $E^i_\perp$, with respect to the external field, $E^e_\perp$:[47−49]

$$E^i_\perp = \frac{2}{\varepsilon_r + 1} E^e_\perp \tag{2}$$

where ε_r is the relative dielectric constant of the cylindrical medium. Instead, the parallel field component is continuous at the interface ($E^i_\parallel = E^e_\parallel$). For $E^e_\perp = E^e_\parallel$, eq 2 gives the attenuation ratio of the perpendicular intensity $\alpha = (I_\perp/I_\parallel) = ((|E^i_\perp|^2)/(|E^i_\parallel|^2)) = (2/(\varepsilon_r + 1))^2$ within the wire. In zincblende InP NWs, where there are no WZ selection rules on band gap transitions, this phenomenon usually yields an emission that can be highly polarized along the NW axis according to eq 2.[50] However, when the absorbed or emitted electromagnetic wave has wavelength comparable to the NW radius a, one has to use the Helmholtz equation and a size dependent polarization degree is found, as reported in refs 48 and 49. Noticeably, for $\omega a/c \approx 0.5$ (where ω is the photon angular frequency, a is the NW radius, and c is the speed of light), a preferential absorption for polarization orthogonal to the NW axis is predicted even for ZB NWs.[48]

Therefore, an estimate of the extent of the dielectric mismatch effect in our NWs and its dependence on the NW geometry is required in order to address the WZ band structure in greater detail. However, such a mismatch cannot be evaluated by PL or PLE measurements in our NWs due to the concomitant presence of polarization-related WZ selection rules. It could be measured in ZB wires with geometrical characteristics identical to our WZ wires, but it is not possible to obtain such pure ZB phase NWs with the same geometry of present WZ phase NWs. Instead, we quantitatively estimate the dielectric mismatch effect by finite-difference time-domain (FDTD) calculations of the ratio between the *absorption* of light polarized parallel and perpendicular to the NW axis, $(I_\parallel/I_\perp)_{calc}$. These calculations are performed for a NW standing up on the InP substrate and illuminated with a plane wave propagating parallel to the substrate surface, as in our measurements (see Figure 2). The shape and dimensions of the NW are those experimentally determined by SEM (see Figure 1a). The calculated $(I_\parallel/I_\perp)_{calc}$ (Figure 4c) decreases with increasing energy, namely, the dielectric mismatch reduces the absorption of perpendicular polarized light, mainly at low energies. By multiplying the PLE spectrum recorded with perpendicular light (blue line in Figure 4a) by the simulated $(I_\parallel/I_\perp)_{calc}$, we essentially filter the dielectric mismatch effect from that spectrum. The approach presented here is a quite general one: The FDTD calculations can be performed for any NW shape and size and for any experimental configuration, that is, with NWs lying or standing up on an arbitrary substrate, and applied to nonaligned NWs provided that polarization-related effects are geometrically averaged over the NW orientation distribution.[51] The resulting PLE spectrum (Figure S4 in the Supporting Information) can now be compared with the one recorded with parallel light. By virtue of the WZ selection rules alone, one gets $I_\perp/I_\parallel \sim 40$ for the A transition, $I_\perp/I_\parallel \sim 4$ for B transition, and $I_\perp/I_\parallel \sim 0.4$ for C transition, after subtraction of the pertinent continua. These results can be directly compared with the ones predicted for WZ-phase materials, as summarized in Figure 4b. The very high anisotropy we find for transition A agrees with the A selection rule. The significant but smaller anisotropy of transition B suggests a considerable perturbation by the spin−orbit effect, as parallel polarized light absorption at and beyond transition B is allowed only by this effect. On the other hand, the slightly lower and opposite anisotropy for transition C can be accounted for by a comparable or slightly larger spin−orbit coupling. Therefore, the measured polarized absorption spectra substantiate the WZ selection rules given in the table. In particular, we point out again that the nearly constant value of $I_\perp/I_\parallel$ between A and B resonances indicates that the optical selection rule of the A transition is maintained for transitions at $k \neq 0$. This issue was considered theoretically in ref 14, and the present results provide an experimental guidance to calculations of the electronic and optical properties of NWs. The contribution of transitions other than those at the Γ point (and their strength evaluation), in fact, gives valuable information about the nonparabolicity of the conduction and valence bands and is also relevant for light detecting devices since most of the absorption processes take place at $k \neq 0$.

The polarized PLE spectra are then used to calculate the absorption degree of polarization, ρ_{abs}, as defined in eq 1. Figure 5a shows the dependence of ρ_{abs} (thick line) on excitation energy for the data displayed in Figure 4a. ρ_{abs} is positive over the entire energy range studied and mirrors the three-step structure of the PLE spectra. It is at a maximum at the perpendicular polarized transition A (=0.86), decreases to =0.60 as the less polarized transition B is activated, and reaches its minimum (=0.28) at energies higher than that of the

DOI: 10.1021/nl5038374
Nano Lett. XXXX, XXX, XXX−XXX

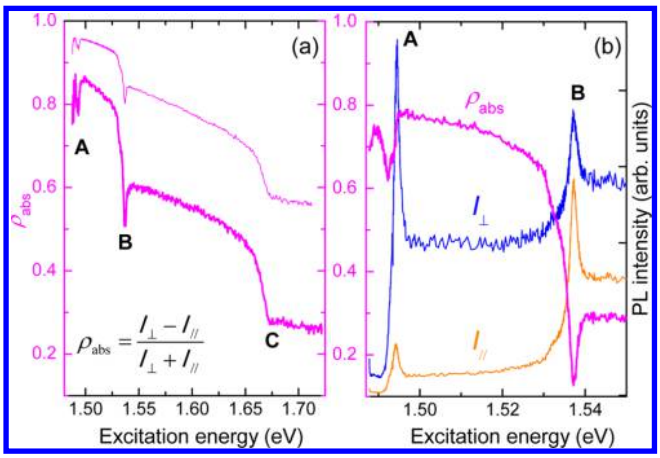

Figure 5. (a) The thick line is the degree of linear polarization ρ_{abs} of absorbed light calculated by applying eq 1 to the two PLE spectra in Figure 4a. A, B, and C transitions are indicated. Notice the two dips in ρ_{abs} at the A and B exciton resonances. The thin line shows the degree of linear polarization after the dielectric mismatch has been filtered out, namely, when $I_\perp$ values have been corrected by FDTD simulations. Here, ρ_{abs} varies from 0.96 to 0.58 when going from A to C, instead of from 0.86 to 0.28 while the three-step feature is maintained. (b) In order to provide more statistics, additional PLE spectra—taken at T = 10 K (E_{det} = 1.487 eV) from a different part of the sample—are shown. PLE spectra excited by light polarization vector parallel and perpendicular to the NW symmetry axis are given by orange and blue lines, respectively, and the resulting ρ_{abs} is given by the pink line. Two dips in ρ_{abs} similar but deeper than those in panel a are clearly observed. In all these and other repeated measurements, the A dip is shifted toward lower energy with respect to the energy of the A exciton resonance in the PLE spectra, whereas the energy of the B dip is equal to that of the B exciton peak in PLE.

oppositely polarized transition C. Two sharp dips (to be discussed in detail later) are also observed to correspond with the A and B exciton resonances in the PLE spectra. Henceforth, they will be referred to as A and B dips.

It should be noted that the values of ρ_{abs} (as well as the absolute $I_\perp$ and $I_{||}$ values) may depend on the alignment of the laser beam with respect to the NW axis. To improve statistical confidence on this issue, a dozen of similar measurements were performed on different parts of the sample and on different samples grown under the same conditions. In any case, the qualitative dependence on excitation energy of $I_\perp$, $I_{||}$, and of the resulting ρ_{abs}, as well as the A, B, and C transition energies, do not depend on sample position or setup alignment. We also stress that the three-plateau feature of ρ_{abs} can be explained solely in terms of the WZ selection rules, as the dielectric mismatch only reduces the absolute value of the measured ρ_{abs} and *monotonically* increases its dynamic range (min-to-max difference). In fact, when the dielectric mismatch is filtered out, namely, when ρ_{abs} is calculated using $I_\perp$ values that are corrected by FDTD simulations, we obtain the energy dependence of ρ_{abs} displayed as thin line in Figure 5a. Therein, the absorption polarization degree varies from 0.96 to 0.58 when going from A to C, instead of from 0.86 to 0.28, while the three-step feature is still maintained. Remarkably, the PLE spectra, as well as the absorption polarization degree, preserve their step-like characteristic up to room temperature for backscattering and grazing incidence. This is detailed in Figure S5 of the Supporting Information.

Exciton Effects on the Absorption Polarization Degree. Let us now discuss the two sharp dips in the absorption degree of polarization displayed in Figure 5a. Figure 5b shows a close-up of the A and B dips appearing in ρ_{abs} (pink line) as determined by polarized PLE spectra taken from a different point of the same NW sample. Here, ρ_{abs} is at a maximum just above transition A (=0.78) and decreases to =0.30 above transition B (the correction introduced by FDTD simulations would give ρ_{abs} =0.93 at A and =0.68 at B). Despite some similarities, the A and B dips show different characteristics in all the cases we have investigated, thus suggesting they should have different origins. In Figure 5b, the line width (~1.5 meV) and peak energy (1.537 eV) of the B dip are exactly the same as those of the B exciton in the PLE spectra. Therefore, the origin of the B dip is quite intuitive. Due to the WZ selection rules, ρ_{abs} is very high when only transitions from the A valence band are activated, whereas at and above the B edge, the less polarized contribution from the B valence band to the PLE signal causes a drop in ρ_{abs}. This drop is deeper at the exciton resonance, where the B contribution is indeed locally higher, thus giving rise to the B dip. For the same reason, no dip is observed at the energy of the C edge, where exciton features are missing in the PLE spectra. On the other hand, the A dip cannot be explained in the same way for at least two reasons: (i) there is no other, less polarized transition in the energy range of the A edge and (ii) the A dip is slightly broader and shifted toward lower energies with respect to the A exciton peak in PLE.

We propose the following explanation for the A dip. We model the A exciton contribution to the complex permittivity $\tilde{\varepsilon}$ of the medium via a simple Lorentz oscillator[52] that results in a resonance in the imaginary part of the permittivity, ε_2, at the exciton energy, whereas the real part, ε_1, has a maximum at an energy just below that of the ε_2 (or absorption) peak; see Figure 6a and paragraph S6 in the Supporting Information. Here, for simplicity reasons and owing to the narrow energy range considered (~20 meV), we neglect the dependence of $\tilde{\varepsilon}$ on frequency originating from the dielectric contrast shown in Figure 4c. Instead, we assume eq 2 to be valid, where we replace ε_r with the energy-dependent ε_1 shown in Figure 6a; details of the parameters chosen in the Lorentz model can be found in paragraph S6 of the Supporting Information. The contribution of the exciton enhancement factor to ε_1 in a semiconductor was first derived analytically by C. Tanguy,[53] who found a maximum in ε_1 slightly below the exciton energy, as in our approach. Tanguy's model was later experimentally verified in different materials.[54−56] In turn, we expect that an enhancement in ε_1 will give rise to an increase in the dielectric mismatch able to produce a dip in the absorption polarization degree. Indeed, the energy dependence of ε_1 in Figure 6a implies, via eq 2, a steep variation in the energy dependence of the dielectric mismatch and in the attenuation ratio $\alpha(E) = I_\perp/I_{||} = [(2)/(\varepsilon_1(E)+1)]^2$. ρ_{abs} can be simulated, therefore, by setting $I_\perp = \alpha(E)\cdot\beta\cdot I_{||}$, where $\alpha(E)$ takes into account the intensity attenuation for perpendicular light polarization due to the dielectric mismatch and β (treated as a free parameter) accounts for the ratio between $I_\perp$ and $I_{||}$ due to WZ selection rules (refer to paragraph S6 in the Supporting Information). One finds

$$\rho_{abs} = \frac{I_\perp - I_{||}}{I_\perp + I_{||}} = \frac{\alpha(E)\beta I_{||} - I_{||}}{\alpha(E)\beta I_{||} + I_{||}} = \frac{\alpha(E)\beta - 1}{\alpha(E)\beta + 1} \quad (3)$$

which is shown in Figure 6b. In Figure 6c, the blue and pink lines are the measured ρ_{abs} displayed in Figure 5a and b,

DOI: 10.1021/nl5038374
Nano Lett. XXXX, XXX, XXX−XXX

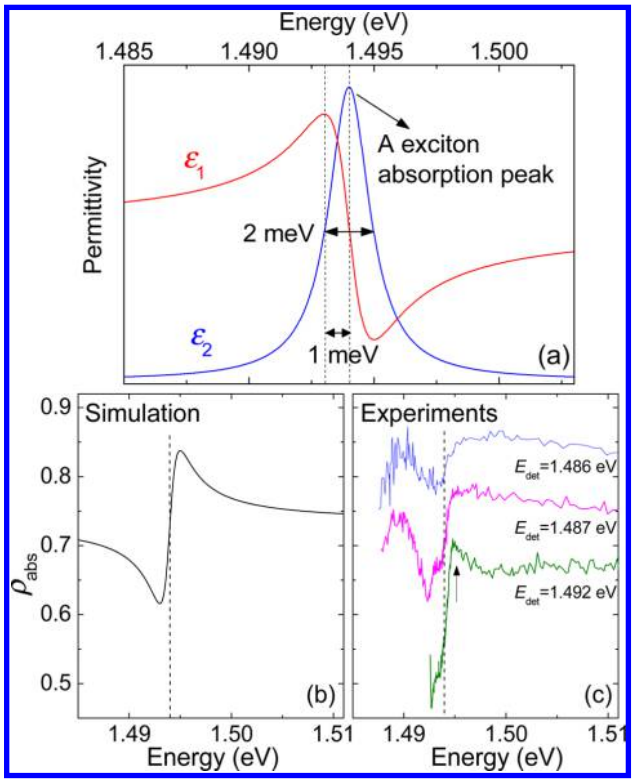

Figure 6. (a) Real (ε_1, red) and imaginary (ε_2, blue) part of the permittivity calculated in the framework of a Lorentz model for a single oscillator representing the exciton resonance. The model parameters have been taken from the experimental width and peak energy of the A exciton as observed in the PLE spectra displayed in Figure 4a and 5b. (b) Degree of polarization calculated by eq 3 using the Lorentz model. The $(I_\perp/I_\parallel)$ energy variation has been derived according to eq 2 by using ε_1 values from panel a. (c) Blue and pink lines show a close-up view of the ρ_{abs} values already displayed in Figure 5a and b, respectively. The green line shows ρ_{abs} as obtained from a different PLE data set —recorded by detecting PL at the FE energy E_{det} = 1.492 eV. A small peak at an energy value just higher than that of the FE energy can be noticed (see arrow). Dashed lines in panels b and c indicate the energy of the A peak in PLE spectra. The simulated and measured shifts (~1 meV) between the A peak and the A dip are in excellent agreement.

whereas the green line shows ρ_{abs} as obtained from PLE spectra (not shown here) recorded by setting the detection energy very close to the FE energy (E_{det} = 1.492 eV). The simulation based on the Lorentz model and shown in Figure 6b reproduces the main observed features of the A dip: (i) its depth, (ii) its line width, which is slightly broader than the corresponding absorption peak (see Figure 5b), and (iii) its energy shift with respect to the A exciton (highlighted by the dashed line in Figure 6c). It is important to mention that the frequency dependence of the refractive index (namely, of the permittivity) at the absorption threshold is significant for several possible optoelectronic applications of nanowires, such as lasers. To this regard, the absorption polarization degree not only is a "spectroscopic curiosity" but also is a sensitive monitoring tool of the energy variation of the NW optical constants.

We would like to stress that our simplified model takes into account only the exciton contribution to the absorption. Thus, the model breaks down on the high energy side of the A dip, where the continuum contribution dominates absorption and will likely hinder the observation of the peak just above the dip displayed in the simulation (Figure 6b). Yet, a tiny increase in ρ_{abs} appears on the high-energy side of the exciton resonance when PLE is measured resonantly at the FE energy (green line in Figure 6c), which further endorses our explanation of the A dip. Likewise, the dominating continuum contribution, along with the much stronger superimposed B dip (already discussed) can screen the analogous feature expected just below the B resonance. Interestingly, two dips with characteristics very similar to those discussed here were also observed in the absorption degree of polarization of WZ GaAs NWs,[15] thus indicating a general character for the phenomenology we reported.

CONCLUSIONS

We performed high-resolution polarization-resolved photoluminescence excitation measurements on a dense ensemble of pure wurtzite-phase InP nanowires. The good optical and structural quality of the samples, together with the suitable procedure developed to deconvolute the macroscopic (i.e., optical) and microscopic (i.e., electronic) contributions to the absorption spectra, allowed us to determine the energy and symmetry of the A, B, and C valence bands in the wurtzite phase with unprecedented reliability. We also provide valuable insights into the effective strength of the spin−orbit interaction on the B and C valence bands and into the influence of a finite k vector on the optical transitions involving band A. The dip observed in the absorption degree of polarization below the A absorption edge is explained within a qualitative model based on the causality relationship between the real and imaginary parts of the permittivity. These results allow us to draw a complete picture of the absorption mechanisms occurring in WZ InP NW ensembles that is useful in the design of optoelectronic devices, such as solar cells and photodetectors.

ASSOCIATED CONTENT

Supporting Information

Supporting Information contains optical measurements and modeling. This material is available free of charge via the Internet at http://pubs.acs.org.

AUTHOR INFORMATION

Corresponding Author

*E-mail: antonio.polimeni@roma1.infn.it.

Present Address

[⊥]School of Biosciences, Cardiff University, The Sir Martin Evans Building, Museum Avenue, Cardiff CF10 3AX, Wales, United Kingdom.

Notes

The authors declare no competing financial interest.

ACKNOWLEDGMENTS

M.D.L., M.C., and A.P. acknowledge funding by Sapienza Università di Roma under the "Avvio alla Ricerca 2014", "Ateneo 2012", and "Ateneo 2013" grants, in that order. The Australian authors acknowledge the Australian Research Council for financial support and Australian National Fabrication Facility and Australian Microscopy and Microanalysis Research Facility for providing access to some of the equipment used in this work. L.M.S. acknowledges funding by the National Science Foundation through NSF DMR-1105362.

DOI: 10.1021/nl5038374
Nano Lett. XXXX, XXX, XXX−XXX

REFERENCES

(1) Lu, W.; Lieber, C. M. *J. Phys. D: Appl. Phys.* **2006**, *39*, R387−R406.
(2) Hayden, O.; Agarwal, R.; Lu, W. *Nano Today* **2008**, *3*, 12.
(3) Yang, P.; Yan, R.; Fardy, M. *Nano Lett.* **2010**, *10*, 1529.
(4) Hochbaum, A. I.; Yang, P. *Chem. Rev.* **2010**, *110*, 527−546.
(5) Garnett, E. C.; Brongersma, M. L.; Cui, Y.; McGehee, M. D. *Annu. Rev. Mater. Res.* **2011**, *1*, 269−295.
(6) Borgström, M. T.; Wallentin, J.; Heurlin, M.; Fält, S.; Wickert, P.; Leene, J.; Magnusson, M. H.; Deppert, K.; Samuelson, L. *IEEE J. Sel. Top. Quant. Electron.* **2011**, *17*, 1050−1061.
(7) Joyce, H. J.; Wong-Leung, J.; Yong, C. K.; Docherty, C. J.; Paiman, S.; Gao, Q.; Tan, H. H.; Jagadish, C.; Lloyd-Hughes, J.; Herz, L. M.; Johnston, M. B. *Nano Lett.* **2012**, *12*, 5325−5230.
(8) Wallentin, J.; Anttu, N.; Asoli, D.; Huffman, M.; Aberg, I.; Magnusson, M. H.; Siefer, G.; Fuss-Kailuweit, P.; Dimroth, F.; Witzigmann, B.; Xu, H. Q.; Samuelson, L.; Deppert, K.; Borgström, M. T. *Science* **2013**, *339*, 1057−1060.
(9) Caroff, P.; Bolinsson, J.; Johansson, J. *IEEE J. Sel. Top. Quant. Electron.* **2011**, *17*, 829−846.
(10) De, A.; Pryor, C. E. *Phys. Rev. B* **2010**, *81*, 155210.
(11) Cheiwchanchamnangij, T.; Lambrecht, W. R. *Phys. Rev. B* **2011**, *84*, 035203.
(12) Dacal, L. C. O.; Cantarero, A. *Solid State Commun.* **2011**, *151*, 781−784.
(13) Murayama, M.; Nakayama, T. *Phys. Rev. B* **1994**, *49*, 4710−4724.
(14) Bechstedt, F.; Belabbes, A. *J. Phys.: Condensed Matter* **2013**, *25*, 273201.
(15) De Luca, M.; Lavenuta, G.; Polimeni, A.; Rubini, S.; Grillo, V.; Mura, F.; Miriametro, A.; Capizzi, M.; Martelli, F. *Phys. Rev. B* **2013**, *87*, 235304 and references therein..
(16) Mattila, M.; Hakkarainen, T.; Mulot, M.; Lipsanen, H. *Nanotechnology* **2006**, *17*, 1580.
(17) Mishra, A.; Titova, L. V.; Hoang, T. B.; Jackson, H. E.; Smith, L. M.; Yarrison-Rice, J. M.; Kim, Y.; Joyce, H. J.; Gao, Q.; Tan, H. H.; Jagadish, C. *Appl. Phys. Lett.* **2007**, *91*, 263104.
(18) Gadret, E. G.; Dias, G. O.; Dacal, L. C. O.; de Lima, M. M., Jr.; Ruffo, C. V. R. S.; Iikawa, F.; Brasil, M. J. S. P.; Chiaramonte, T.; Cotta, M. A.; Tizei, L. H. G.; Ugarte, D.; Cantarero, A. *Phys. Rev. B* **2010**, *82*, 125327.
(19) Perera, S.; Pemasiri, K.; Fickenscher, M. A.; Jackson, H. E.; Smith, L. M.; Yarrison-Rice, J.; Paiman, S.; Gao, Q.; Tan, H. H.; Jagadish, C. *Appl. Phys. Lett.* **2010**, *97*, 023106.
(20) Montazeri, M.; Wade, A.; Fickenscher, M.; Jackson, H. E.; Smith, L. M.; Yarrison-Rice, J. M.; Gao, Q.; Tan, H. H.; Jagadish, C. *Nano Lett.* **2011**, *11*, 4329−4336.
(21) Tuin, G. L.; Borgström, M. T.; Tragårdh, J.; Ek, M.; Wallenberg, L. R.; Samuelson, L.; Pistol, M. *Nano Res.* **2011**, *4*, 159−163.
(22) Alouane, M. H. H.; Chauvin, N.; Khmissi, H.; Naji, K.; Ilahi, B.; Maaref, H.; Patriarche, G.; Gendry, M.; C Bru-Chevallier, C. *Nanotechnology* **2013**, *24*, 035704.
(23) Perera, S.; Shi, T.; Fickenscher, M. A.; Jackson, H. E.; Smith, L. M.; Yarrison-Rice, J. M.; Paiman, S.; Gao, Q.; Tan, H. H.; Jagadish, C. *Nano Lett.* **2013**, *13*, 5367−5372.
(24) Li, K.; Sun, H.; Ren, F.; Ng, K. W.; Tran, T.-T. D.; Chen, R.; Chang-Hasnain, C. J. *Nano Lett.* **2014**, *14*, 183−190.
(25) Gao, Q.; Saxena, D.; Wang, F.; Fu, L.; Mokkapati, S.; Guo, Y.; Li, L.; Wong-Leung, J.; Caroff, P.; Tan, H. H.; Jagadish, C. *Nano Lett.* **2014**, *14*, 5206−5211.
(26) De Luca, M.; Polimeni, A.; Fonseka, H. A.; Meaney, A. J.; Christianen, P. C. M.; Maan, J. C.; Paiman, S.; Tan, H. H.; Jagadish, C.; Capizzi, M. *Nano Lett.* **2014**, *14*, 4250−4256.
(27) Vu, T. T. T.; Zehender, T.; Verheijen, M. A.; Plissard, S. R.; Immink, G. W. G.; Haverkort, J. E. M.; Bakkers, E. P. A. M. *Nanotechnology* **2013**, *24*, 115705 1−6.
(28) Wallentin, J.; Anttu, N.; Asoli, D.; Huffman, M.; Åberg, I.; Magnusson, M. H.; Siefer, G.; Fuss-Kailuweit, P.; Dimroth, F.; Witzigmann, B.; Xu, H. Q.; Samuelson, L.; Deppert, K.; Borgström, M. T. *Science* **2013**, *339*, 1057.
(29) Yoshimura, M.; Nakai, E.; Tomioka, K.; Fukui, T. *Appl. Phys. Lett.* **2013**, *103*, 243111.
(30) De Luca, M.; Polimeni, A.; Capizzi, M.; Meaney, A. J.; Christianen, P. C. M.; Maan, J. C.; Mura, F.; Rubini, S.; Martelli, F. *ACS Nano* **2013**, *7*, 10717.
(31) Kupec, J.; Stoop, R. L.; Witzigmann, B. *Opt. Expr.* **2010**, *18*, 27589.
(32) Anttu, N.; Xu, H. Q.; Nanosci, J. *Nanotechnology* **2010**, *10*, 7183−7187.
(33) De Luca, M.; Polimeni, A.; Felici, F.; Miriametro, A.; Capizzi, M.; Mura, F.; Rubini, S.; Martelli, F. *Appl. Phys. Lett.* **2013**, *102*, 173102.
(34) Iqbal, A.; Beech, J. P.; Anttu, N.; Pistol, M. E.; Samuelson, L.; Borgström, M. T.; Yartsev, A. *Nanotechnology* **2013**, *24*, 115706.
(35) Paiman, S.; Gao, Q.; Joyce, H. J.; Kim, Y.; Tan, H. H.; Jagadish, C.; Zhang, X.; Guo, Y. *J. Appl. Phys. D* **2010**, *43*, 445402.
(36) Gudiksen, M. S.; Wang, J.; Lieber, C. M. *J. Phys. Chem. B* **2002**, *106*, 4036−4039.
(37) Diedenhofen, S. L.; Janssen, O. T. A.; Grzela, G.; Bakkers, E. P. A. M.; Rivas, J. G. *ACS Nano* **2011**, *5*, 2316−2323.
(38) Fan, Z.; Kapadia, R.; Leu, P. W.; Zhang, X.; Chueh, Y.-L.; Takei, K.; Yu, K.; Jamshidi, A.; Rathore, A. A.; Ruebusch, D. J.; Wu, M.; Javey, A. *Nano Lett.* **2010**, *10*, 3823.
(39) Yu, P. Y.; Cardona, M. *Fundamentals of Semiconductors*, 3rd ed.; Springer: Berlin, 2005; Chapter 7, p 369.
(40) Koteles, E. S.; Lee, J.; Salerno, J. P.; Vassell, M. O. *Phys. Rev. Lett.* **1985**, *55*, 867.
(41) Benzaquen, R.; Leonelli, R.; Charbonneau, S. *Phys. Rev. B* **1999**, *59*, 1973−1985.
(42) Kim, D. C.; Dheeraj, D. L.; Fimland, B. O.; Weman, H. *Appl. Phys. Lett.* **2013**, *102*, 142107.
(43) Efros, Al. L.; Lambrecht, W. R. L. *Phys. Rev. B* **2014**, *89*, 035304.
(44) Birman, J. L. *Phys. Rev.* **1959**, *114*, 1490.
(45) Polimeni, A.; Patanè, A.; Grassi Alessi, M.; Capizzi, M.; Martelli, F.; Bosacchi, A.; Franchi, S. *Phys. Rev. B* **1996**, *54*, 16389−16392.
(46) Tronc, P.; Kitaev, Y. E.; Wang, G.; Limonov, M. F.; Panfilov, A. G.; Neu, G. *Phys. Status Solidi B* **1999**, *216*, 599.
(47) Landau, L. D.; Lifshitz, E. M.; Pitaevskii, L. P. *Electrodynamics of Continuous Media*; Pergamon: Oxford, 1984; pp 34−42.
(48) Ruda, H. E.; Shik, A. *J. Appl. Phys.* **2006**, *100* (024314), 1−6.
(49) Chen, H.-Y.; Yang, Y.-C.; Lin, H.-W.; Chang, S.-C.; Gwo, S. *Opt. Express* **2008**, *16*, 13465−13475.
(50) Wang, J.; Gudiksen, M. S.; Duan, X.; Cui, Y.; Lieber, C. M. *Science* **2001**, *293*, 1455−1457.
(51) Fang, L.; Zhao, X.; Chiu, Y.-H.; Ko, D.; Reddy, K. M.; Lemberger, T. R.; Padture, N. P.; Yang, F.; Johnston-Halperin, E. *Appl. Phys. Lett.* **2011**, *99*, 141101 1−3.
(52) Saleh, B. E. A.; Teich, M. C. *Fundamentals of Photonics*, 2nd ed.; John Wiley & Sons Inc.: Hoboken, NJ, 2007; Chapter 5.
(53) Tanguy, C. *Phys. Rev. Lett.* **1995**, *75*, 4090−4093.
(54) Tanguy, C. *IEEE J. Quantum Electron.* **1996**, *32*, 1746−1751.
(55) Safonova, L.; Brazis, R.; R. Narkowicz, R. *Lith. J. Phys.* **2004**, *44*, 421−425.
(56) Marquezini, M. V.; Tignon, J.; Hasche, T.; Chemla, D. S. *Appl. Phys. Lett.* **1998**, *73*, 2313−2315.

DOI: 10.1021/nl5038374
Nano Lett. XXXX, XXX, XXX−XXX